Received: 22 February 2023 | Revised: 1 July 2023 | Accepted: 5 July 2023

DOI: 10.1002/brx2.25

RESEARCH ARTICLE

Brain-X Open Access WILEY

Target localization intervention and prognosis evaluation for an individual with mild cognitive impairment

Weiping Wang[1,2,3] | **Haiyan Zhao**[4] | **Chang He**[1,2,3] | **Yuanbo Cui**[5] | **Zhen Wang**[6] | **Alexander Hramov**[7,8] | **Ping Luan**[9] | **Xiong Luo**[1,2,3] | **Jipeng Ouyang**[10] | **Kurths Jürgen**[11,12]

[1]School of Computer and Communication Engineering, University of Science and Technology Beijing, Beijing, China

[2]Shunde Graduate School, University of Science and Technology Beijing, Foshan, Guangdong, China

[3]Beijing Key Laboratory of Knowledge Engineering for Materials Science, Beijing, China

[4]Department of Neurology, Peking University Third Hospital, Beijing, China

[5]The 6th Research Institute of China Electronics Corporation, Beijing, China

[6]The Center for Optical Imagery Analysis and Learning and School of Mechanical Engineering, Northwestern Polytechnical University, Xi'an, Shaanxi, China

[7]Center for Technologies in Robotics and Mechatronics Components, Innopolis University, Innopolis, Russia

[8]Saratov State Medical University, Saratov, Russia

[9]Guangdong Second Provincial General Hospital & Health Science Center, Shenzhen, Guangdong, China

[10]Department of Neurology, Shunde Hospital, Southern Medical University, Foshan, Guangdong, China

[11]Institute of Physics, Humboldt-University, Berlin, Germany

[12]Potsdam Institute for Climate Impact Research, Potsdam, Germany

Correspondence

Zhen Wang, The Center for Optical Imagery Analysis and Learning and School of Mechanical Engineering, Northwestern Polytechnical University, Xi'an, Shaanxi 710072, China.
Email: nkzhenwang@163.com

Chang He, School of Computer and Communication Engineering, University of Science and Technology Beijing, Beijing 100083, China.
Email: 15603293375@163.com

Abstract

Currently, no specific treatments are available for Alzheimer's disease (AD). Mild cognitive impairment (MCI), the preclinical stage of AD, has a high possibility of reversing symptoms through neural regulation. A state dynamics model for single brain regions was developed to simulate blood oxygen level-dependent signals in a patient with early mild cognitive impairment. Subsequently, the analysis of functional connections was used to comprehensively consider multiple complex network centralities to locate the intervention targets, and a multiple brain region collaborative control scheme was designed. Finally, the reliability and effectiveness of the intervention were verified at the brain region and subnetwork levels. This

Funding information: National Science Fund for Distinguished Young Scholarship of China, Grant/Award Number: 62025602; Ministry of Industry and Information Technology Special Fund for High-Quality Development, Grant/Award Number: TC220A04A-182; Science and Technology Innovation Special Foundation of Foshan Municipal Peoples Government, Grant/Award Number: BK21BFO01; XPLORER PRIZ; Fundamental Research Funds for the Central Universities, Grant/Award Number: QNXM20220038; Key Project of Basic Research of Shenzhen, Grant/Award Number: JCYJ20200109113603854; National Natural Science Foundation of China, Grant/Award Number: 62271045; Innovation and Transformation Foundation of Peking University Third Hospital, Grant/Award Number: BYSYZHKC2021107; Key Technology Research and Development Program of Science and Technology-Scientific and Technological Innovation Team of Shaanxi Province, Grant/Award Number: 2020TD-013

Weiping Wang and Haiyan Zhao contributed equally to this work, and they are co-first authors.

technique provides a basis for future clinical diagnosis and treatment of AD and MCI.

KEYWORDS
adaptive pinning control, Alzheimer's disease, BOLD signals, computational modeling, Sub_network

1 | INTRODUCTION

Alzheimer's disease (AD) is a heterogeneous disease with an unclear etiology, and currently, no specific AD treatments are available. Mild cognitive impairment (MCI), the early stage of AD, can be divided into early MCI (EMCI) and late MCI (LMCI).[1] Patients with MCI experience mild cognitive decline, but their daily activities are not substantially affected. Therefore, these patients often control and inhibit the progression of MCI with drug therapy, traditional Chinese medicine,[2] cognitive training,[3] and external stimulation therapy.[4]

The presentation of MCI varies greatly among patients; therefore, patients' treatment plans must be customized for their cognitive recovery. Successful recovery is based on a full understanding of the brain. Resting-state magnetic functional resonance imaging (fMRI)[5] and diffusion tensor imaging (DTI)[6] can capture information on brain functional networks and structural networks, providing basic tools for studying brain diseases; in addition, neural computational modeling provides an effective method to achieve a complete understanding of the brain. Several data-driven models have been proposed to describe temporal state changes in specific brain regions and the whole brain. Deco[7] and Demirtas et al.[8] used the normal form of a Hopf bifurcation to simulate the state changes of a single brain node and analyzed the changes in resting-state functional connectivity (FC) in the whole brain during AD progression. The dynamic causal model (DCM), a directed model, can describe differences in neuronal signals over time, providing a powerful and intuitive analytical tool for functional network simulation based on structural networks.[9,10]

Most existing control schemes use state reproduction to adjust the system state by directly adjusting the parameter values in the model.[11] The control parameters cannot be automatically adjusted in real-time according to the status of the nodes and the system. In addition, because all nodes in the brain are treated as control objects without differences, low-level trauma cannot be achieved. Therefore, to control the human brain with minimal damage and high flexibility, the adaptive pinning control scheme can be used to improve brain FC in the resting state and enhance cognitive ability in patients.

Sufficient and convincing cognitive recovery criteria play a key role in cognitive recovery. Depending on the focus of the study, FC and functional connectivity dynamics are often selected to measure the brain state.[12,13] The internal and external connections of functional subnetworks have a substantial effect on individual cognitive performance.[14,15,16] For example, the default mode network (DMN) is composed of the posterior cingulate cortex, precuneus, medial prefrontal cortex, inferior parietal lobe, bilateral temporal cortex, and other brain regions. It is believed to be closely related to the functions of the human brain, such as the monitoring of the internal and external environment, emotional processing, introspection, and episodic memory retrieval.[17,18] Therefore, a comprehensive analysis of the connectivity inside and outside the subnetwork and FC can be used to evaluate the effect of cognitive recovery programs at multiple levels.

Key points

What is already known about this topic?

- Preprocessing various structural and neuroimaging data can reveal the structure of the brain and functional network as well as the related functional activity information in mild cognitive impairment (MCI) patients.

What does this study add?

- According to a precise simulation of individual brain region activities, the proposed method of coordinated adaptive control of multiple brain regions could restore cognitive ability in MCI patients by positioning a pinning target in the deep brain, providing theoretical guidance for personalized clinical neuroregulation.

To explore the brain network mechanism in patients with MCI and AD and provide guidance for intervention targets of future clinical interventions, this study simulated blood oxygen level-dependent (BOLD) signals in patients with EMCI via the DCM, designed a multiple brain region collaborative adaptive intervention scheme, and explored the recovery effect at the brain region and subnetwork FC levels. The patient-specific cognitive recovery framework is shown in Figure 1 and the specific contributions of this paper are as follows:

1. Through DCM deformation, we accurately simulated the BOLD signal in each brain region of individuals with EMCI to capture the neural activity and disease evolution of each patient.

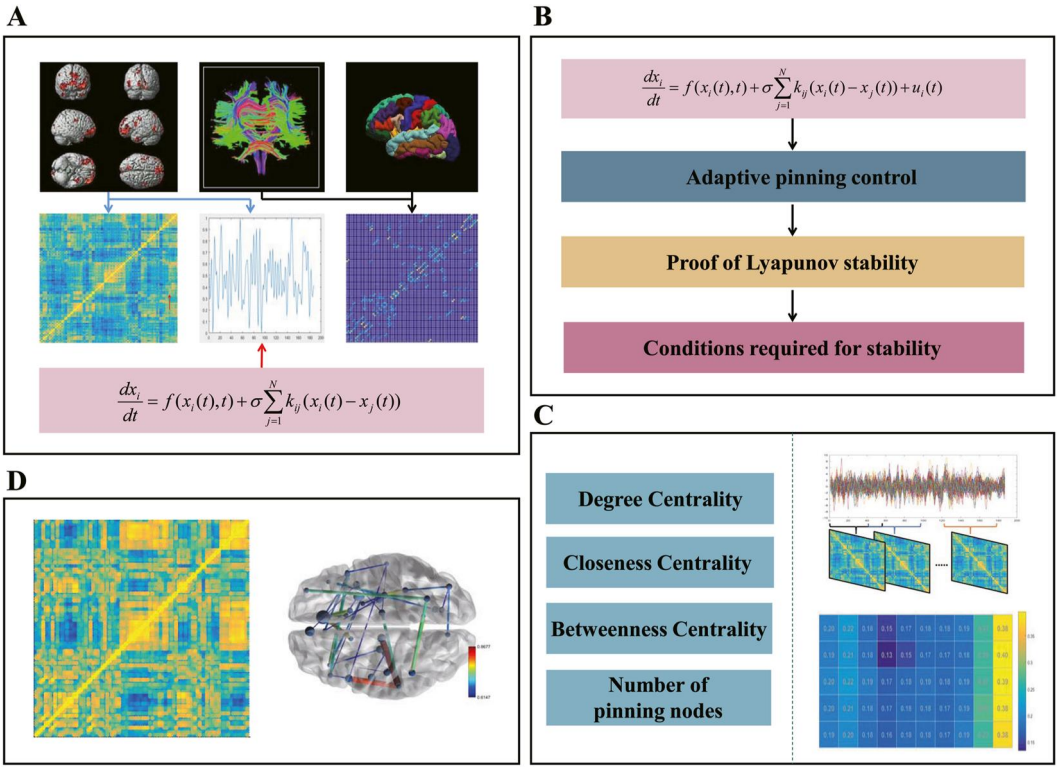

FIGURE 1 Patient-specific cognitive recovery framework based on multiple brain region collaboration. (A) Image preprocessing. FMRI data were processed by the DPARSF to obtain FC and the BOLD signals of each brain region. DTI and T1 images were processed by MRtrix3 to obtain SCs. The FC and BOLD signals were simulated by substituting SC into the model and adjusting the specific parameters *Pij* and σ. (B) Design and stability proof of the adaptive pinning control scheme. (C) Pinning node and time segment selection strategy. The pinning nodes were selected on the basis of the centralities of the complex network, and the potential impact of the number of pinning nodes was considered. A sliding window was used, and an algorithm was designed to calculate the difference between FCs to select the target time segment. (D) Theoretical recovery effect. The effect was discussed from the perspectives of FC strength and subnetwork connectivity distribution. BOLD, blood oxygen level-dependent; DPARSF, data processing assistant for resting-state fMRI; DTI, diffusion tensor imaging; FC, functional connectivity; fMRI, functional magnetic resonance imaging; NC, normal control; SC, structural connectivity.

2. Pinning nodes were determined according to multiple centralities of the complex network, and the average FC difference between the control group and the individual was calculated using a sliding window at multiple steps. Subsequently, the controlled time periods were selected to design an adaptive multiple brain region collaborative control scheme to provide a method for future clinical interventions for specific patient conditions.
3. The cognitive recovery effect was evaluated at two levels: the brain area and the functional subnetwork-related connections. The stronger and weaker connections between individuals and the control groups were compared at the brain area level, and the distribution of inward and outward connections was compared at the functional subnetwork level. The multilevel FC evaluation scheme may provide ideas for patients' cognitive ability evaluation based on functional imaging.

The remainder of this paper is organized as follows: Section 2 introduces the data collection and processing process, the computational model and the multiple brain region collaborative control scheme, and the other materials and methods required for the experiment. The theoretical simulation results of the control scheme are provided in Sections 3 and 4, which demonstrate the effectiveness of the proposed strategy and discuss the results, respectively.

2 | MATERIAL AND METHODS

2.1 | Participants

A 75-year-old female and an 80-year-old male with EMCI were selected as participants. For each participant, two control groups of 10 healthy individuals aged 70–86 were created. All patients underwent clinical symptom examinations, neuropsychological tests, neuroimaging examinations, and biomarker detection. The first and second control groups for the female participant had a male-to-female ratio of 1:1 and 0:1, respectively, and the male participant's control groups had a male-to-female ratio of 1:1 and 1:0. Detailed data are shown in Table 1, which were obtained from the Alzheimer's Disease Neuroimaging Initiative Database (ADNI, https://adni.loni.usc.edu). All participants underwent resting-state fMRI (BOLD sensitive, T2*-weighted, TR 3000 ms, TE 30 ms, FA 90,197 slices [3.4 mm]), structural magnetic resonance imaging, and DTI (slice thickness 2 mm, TE 56 ms, TR 7200 ms, 54 directions, b = 1000 s = mm^2).

TABLE 1 Participant demographics.

Subject	Group	Sex	Age
068_S_2315	EMCI	F	78
002_S_1261	NC	F	82
002_S_1280	NC	F	81
002_S_6007	NC	F	77
011_S_6367	NC	F	82
014_S_6988	NC	F	83
002_S_4213	NC	F	84
003_S_4288	NC	F	78
011_S_4105	NC	F	77
014_S_4576	NC	F	76
014_S_6148	NC	F	82
002_S_4473	EMCI	M	80
002_S_4225	NC	M	77
003_S_4350	NC	M	81
011_S_4278	NC	M	83
014_S_6437	NC	M	79
032_S_6294	NC	M	82
002_S_6456	NC	M	86
003_S_6259	NC	M	71
003_S_6307	NC	M	76
003_S_6644	NC	M	86
032_S_6717	NC	M	75

2.2 | Image acquisition and preprocessing

Statistical parametric mapping software with the Data Processing Assistant for Resting-State fMRI[19] software package (http://rfmri.org/content/dparsf) was used to preprocess the fMRI data. First, the data were converted from Digital Imaging and Communications in Medicine format to Neuroimaging Informatics Technology Initiative format, and the data from the first 10 time points for each object were discarded. Subsequently, hierarchical correction and head movement correction were performed, and the data were registered in the same space for downsampling. Interfering signals were removed from the time series of each voxel to reduce the effect of nonneuronal fluctuations. Bandpass filtering was used to filter the time series from 0.04 to 0.07 Hz, and the brain was divided into 90 brain regions according to the automated anatomical labeling (AAL) template. Finally, the time series of all brain regions of each object were obtained by averaging the time series of all voxels in a specific region of interest.

In MRtrix3 (https://www.mrtrix.org/) software, the dwidenoise function was used to denoise the data, and the dwifslPreproc function was used to preprocess them.[20] The operations performed were susceptibility-induced distortion, eddying current-induced distortion, and motion effect. After $b0$ was extracted, the mask was generated, the image was standardized, and the T1 image was preprocessed and registered with the DTI image. The dwi2response, dwi2fod, and tckgen functions were used to track the whole brain fiber, and then sift correction was performed. Finally, a 90×90 structural connection matrix was estimated according to the number of streamlines connecting each pair of regions.

2.3 | Computational model design for single-brain BOLD signal simulation

The DCM can adjust the prediction results of the Bayesian model and realize the conversion from neural activity to BOLD signals by establishing an interaction model of neural activity in the brain and a hemodynamic model of each brain region so that the differential equation of neuronal activity fits the brain imaging data. Erik et al.[21] used the dynamic causal modeling neuronal state equation to simulate the transmission process of neural activity along the structural connections of the nervous system. The model they derived is as follows:

$$\frac{dx_i}{dt} = f(x, v, \theta) + \sigma \sum_{j=1}^{N} k_{ij}\left(x_i - x_j\right), \tag{1}$$

where $N = 90$ is the number of the brain regions; x_i and x_j represent the ith and jth signals, respectively; σ is the diffusion coefficient, which controls the rate at which neuronal fluctuations spread to neighboring areas; k_{ij} is the structural connection strength of the brain regions, which can be obtained by image processing; and v and θ represent the stimulus parameter and hyperparameter, respectively.

Assuming first-order interactions, Equation (1) can be linearized to Equation (2), which can be written as follows:

$$\frac{dx_i}{dt} = \sum_{j=1}^{N} p_{ij} x_j(t) + \sigma \sum_{j=1}^{N} k_{ij}\left(x_i(t) - x_j(t)\right) + \omega^{(i)}, \tag{2}$$

for which a detailed explanation of the parameters can be found in Ref. [21].

A. Design and stability analysis of adaptive pinning control scheme.

The controlled network is described as follows:

$$\frac{dx_i}{dt} = f(x, v, \theta) + \sigma \sum_{j=1}^{N} k_{ij}\left(x_i(t) - x_j(t)\right) + u_i(t), \tag{3}$$

where $u_i(t)$ is the control strength of the ith node. The adaptive pinning control scheme was chosen as the control scheme; $u_i(t)$ is defined as:

$$u_i(t) = \begin{cases} c_i(t)(s_i(t) - x_i(t)), 1 \le i \le l, \\ 0, l+1 < i \le N. \end{cases} \tag{4}$$

where l is the number of the pinning nodes, $s_i(t)$ is the desired state of the ith brain region, and $c_i(t)$ is the control gain. The error variable of the ith node can be defined as $e_i(t) = x_i(t) - s_i(t)$. Then, the error dynamic formula can be written as

$$\begin{cases} \dot{e}_i(t) = f(x_i(t), t) - f(s_i(t), t) + \sigma \sum_{j=1}^{N} k_{ij}\left(x_i(t) - x_j(t)\right) + c_i(s_i(t) - x_i(t)) \\ i = 1, 2, 3, ..., l, \\ \dot{e}_i(t) = f(x_i(t), t) - f(s_i(t), t) + \sigma \sum_{j=1}^{N} k_{ij}\left(x_i(t) - x_j(t)\right) \\ i = l+1, l+2, ..., N. \end{cases} \tag{5}$$

The control gain $c_i(t)$ is defined as

$$\dot{c}_i(t) = k_i(x_i(t) - s_i(t))^T(x_i(t) - s_i(t)), \tag{6}$$

The following assumption was needed to obtain our results.

Assumption 1. Assume that the nonlinear function $f(\cdot)$ satisfies the Lipschitz condition, that is, for any time t, there is a nonnegative constant α:

$$\|f(x_i(t)) - f(s_i(t))\| \le \alpha \|x_i(t) - s_i(t)\|, \tag{7}$$

Remark 1. Many classical chaotic function systems, such as the Lorenz system, Chen system, and Chua system, satisfy the Lipschiz condition, and the neural activity of the human brain also satisfies the chaotic characteristics, so it is assumed that the Lipschiz condition is also satisfied.

Considering that $\sum_{j=1}^{N} k_{ij}\left(x_i(t) - x_j(t)\right)$ can be derived and reduced to $\sum_{j=1}^{N} l_{ij}x_j(t)$,[21] where l_{ij} is the Laplacian matrix.

Proof. The Lyapunov functional candidate is defined as

$$V(t) = \frac{1}{2}\sum_{i=1}^{N} e_i(t)^T e_i(t) + \frac{1}{2}\sum_{i=1}^{N} \frac{(c_i(t) - m)^2}{k_i}, \tag{8}$$

where m is a sufficiently large normal number. Differentiating $V(t)$ gives:

$$\begin{aligned} \dot{V}_i(t) &= \sum_{i=1}^{N} e_i(t)^T(f(x_i(t), t) - f(s_i(t), t)) + \sigma \sum_{i=1}^{N}\sum_{j=1}^{N} k_{ij} e_i(t)^T\left(x_i(t) - x_j(t)\right) \\ &\quad + \sum_{i=1}^{N} c_i(t) e_i(t)^T(s_i(t) - x_i(t)) + \sum_{i=1}^{l}(c_i(t) - m) e_i(t)^T e_i(t) \\ &= \sum_{i=1}^{N} e_i(t)^T(f(x_i(t), t) - f(s_i(t), t)) + \sigma \sum_{i=1}^{N}\sum_{j=1}^{N} k_{ij} e_i(t)^T\left(x_i(t) - x_j(t)\right) \\ &\quad - m\sum_{i=1}^{l} e_i(t)^T e_i(t) \\ &\le \alpha \sum_{i=1}^{N} e_i(t)^T e_i(t) + \sigma \sum_{i=1}^{N}\sum_{j=1}^{N} k_{ij} e_i(t)^T\left(x_i(t) - x_j(t)\right) - m\sum_{i=1}^{l} e_i(t)^T e_i(t) \\ &\le \alpha \sum_{i=1}^{N} e_i(t)^T e_i(t) + \sigma \sum_{i=1}^{N}\sum_{j=1}^{N} l_{ij} e_i(t)^T\left(x_i(t) - x_j(t)\right) - m\sum_{i=1}^{l} e_i(t)^T e_i(t) \\ &\le \alpha e(t)^T e(t) + \sigma L_{\min} e(t)^T e(t) - m e(t)^T e(t) \\ &\le (\alpha + \sigma L_{\min} - m) e(t)^T e(t) \end{aligned}$$

where $L_{\min} = 0$ is the smallest eigenvalue of L. According to the above, it is determined that $\alpha - m < 0$ is the sufficient condition for $\dot{V}(t) \leq 0$. Because the adaptive controller can automatically update the control factor, the controller parameter setting depends only on the dynamic parameters of each brain node.

2.4 | Preliminary preparation of the theoretical experiment

According to the above, the brain state models of the male and the female participants were obtained, and theoretical experiments were carried out to test the cognitive recovery effect of the control scheme. To improve the interpretability and ensure the simulation effect, some of the preliminary preparation of the experiment is described, including the selection of the controlled time series pairs, the determination of the pinning nodes, and the design of the evaluation criteria for functional recovery.

2.4.1 | Selection scheme of controlled BOLD time series pairs

The ADNI database does not record information about specific individuals over a long period, so the male and female participants in the EMCI stage were selected without the multimodal neuroimages collected during normal aging. Therefore, three groups of 10 NC participants in the same age range were selected (i.e., 5 males and 5 females, 10 males and 10 females), and their BOLD signals were averaged to obtain the theoretical target state of the BOLD signals in the three groups in the normal state. Because of the differences in the external environment and the human brain state, it is difficult to directly regard the BOLD signals based on the group average as the target state. Furthermore, the BOLD signal evolution of patients with EMCI cannot be fully explained by the average of the control group because the average initial brain state of the control group is not consistent with that of the patients. Furthermore, the BOLD signals of the EMCI patients cannot be controlled to transform them into a state equal to the average state of the NC group. The key problem is that the initial brain state represented by the BOLD time series is not matched between subjects and controls. In this study, to apply the control to precise time periods and measure the control effect, a difference heterogeneity algorithm was designed to locate the initial locus of the controlled time series in the patients with EMCI and the control groups.

First, we adopted a sliding window approach to cut the BOLD signals of the EMCI patient and averaged the NC, and the time segment length was set to 40 time points. To specify the optimal sampling interval, the sampling interval d was set to 5, 10, 15, and 20 time points sequentially.

Afterward, the Pearson correlation coefficient between each brain region was calculated on the basis of the BOLD signals within each time segment to obtain the FC. The FC of the averaged NC and the patient with EMCI (FC NC and FC EMCI, respectively) were processed with 0.5 as the threshold. If the correlation coefficient was >0.5, it was adjusted to 1; if it was < −0.5, it was adjusted to −1; and the rest were set to 0. The processed FC NC and FC EMCI were compared, and if the values at the same position (the position range was between [0, 0] and [90, 90]) were different, the difference degree was increased by 1, otherwise it was not changed. By traversing, the difference degree between the FCs was obtained.

2.4.2 | Selection scheme of pinning nodes

The location of the pinning node determines the efficiency and effect of the control. The centrality of a complex network can locate the central nodes in the network. Hence, selecting pinning nodes allows high efficiency and low power consumption. According to the structural connection network of the patient obtained by preprocessing, three types of centrality scores of each node in the complex network were comprehensively considered: degree centrality, betweenness centrality, and closeness centrality.

Degree centrality is the most direct measure to describe node centrality in network analysis.[22] The larger the degree of a node, the more important the node is in the network. The degree of the ith node is as follows:

$$C_D(i) = \frac{ki}{N-1}, \tag{10}$$

where k_i is the number of existing edges connected to node i, and $N - 1$ represents the number of edges at which node i is connected to other nodes.

Betweenness centrality refers to the proportion of the number of paths passing through the node in the total number of shortest paths in the network, which reflects the influence of the node in the entire network. A node with a higher value of betweenness centrality takes on heavier information transmission tasks in the network:

$$C_B(i) = \sum_{j<k} \frac{g_{ik}(i)}{g_{ik}}, \tag{11}$$

where $g_{ik}(i)$ represents the paths between j and k that pass through i, and g_{ik} represents all paths between j and k. It can be normalized as follows:

$$C_B^{'}(i) = \frac{C_B(i)}{(n-1)(n-2)/2}, \tag{12}$$

where $(n - 1)(n - 2)/2$ is the number of pairs of vertices, excluding the vertex itself.

Closeness centrality is used to measure node importance, which depends on the inverse distance to other vertices.[23] The node with the largest closeness centrality value is the topology center of the entire network, which is defined as follows:

$$C_C(i) = \left[\sum_{j=1}^{N} d(i,j)\right]^{-1}. \quad (13)$$

It can also be normalized as

$$C_C^{'}(i) = (C_C(i)).(N-1), \quad (14)$$

where $d(i, j)$ represents the distance between node i and node j, and N is the number of nodes in the network.

2.4.3 | Functional recovery assessment criteria

The FC changes in the brain regions and subnetworks were used to measure the effectiveness of the experiment regarding the restoration of brain cognitive function; quantitative results were determined by the statistical analysis method.

The direct control object of the intervention scheme was the BOLD signals in the whole brain. To establish the association with function, Pearson correlation analysis was conducted on the BOLD signal before and after the control, and the changes in the functionally connected brain network were obtained. The purpose of the control was to improve the strength of the weak functional connections between brain regions closely related to cognition and to enhance the information communication between brain regions by maintaining the original specific dominant connections. Thus, brain-wide dominance and disadvantage connections before and after the intervention are also considered.

Increasingly, cognitive neuroresearchers are shifting their focus from isolated brain regions to larger brain networks. According to different research backgrounds and purposes, different brain network classification methods have been used. In this study, following the division of the brain functional network proposed by Yeo,[24] the whole brain was divided into seven subnetworks: the visual network (VN), Somatic motor network, dorsal attention network (DAN), ventral attention network (VAN), limbic network (LN), control network (CN), and DMN. The DAN, VAN, CN, DMN, and LN are strongly correlated with human cognitive ability; therefore, only the above subnetworks were analyzed.[25,26] The research was carried out from two aspects: FC changes within and between subnetworks. Within the subnetwork, the distribution of functional connection strength in brain regions before and after control was compared. More functional connections correspond to more frequent and easier information exchange. Therefore, the number of functional connections related to brain regions that play a key role in external information exchange was also used as one of the criteria.

3 | RESULTS

3.1 | Model-based BOLD signal simulation

The BOLD signals of two EMCI patients are simulated according to the model (3). To select the diffusion coefficient σ, we set the step size 0.05 to fit the experiential signal within the range of [0, 1] and choose 0.15 and 0.95 as the best-fitting values of the diffusion coefficient for the female and the male participants, respectively. The fitting effect is shown in Figure 2.

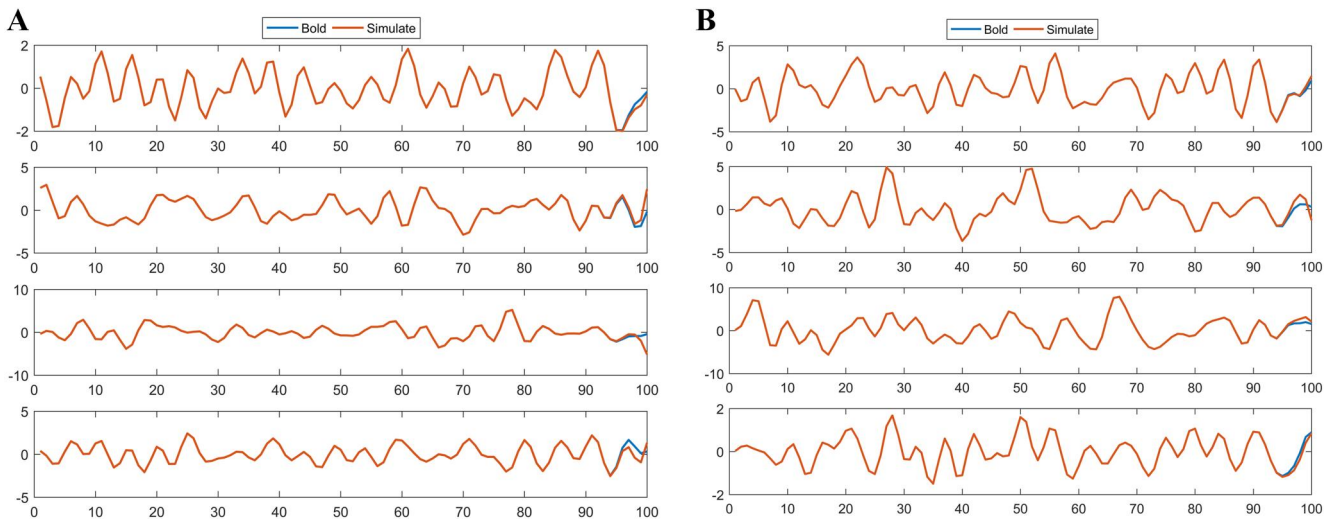

FIGURE 2 The fitting effect of the model to the real signals; brain regions 1, 26, 51, and 76 are represented from top to bottom. (A) Female participant. (B) Male participant.

3.2 | Theoretical control effect

In this section, the selection results of the pinning nodes and the controlled time series pairs are shown first, and then the theoretical recovery effect is evaluated from the aspects of FC connection strength and subnetwork distribution.

3.2.1 | Controlled time series pairs selection

Considering that the external environment and internal brain activity are difficult to replicate, we first selected time segments by comparing the difference between the FC NC and FC EMCI before conducting the control experiment.

For each value of d, we calculated the difference degree and obtained the corresponding difference degree maps. The length of the controlled time segment was set to 100 time points because of the excellent performance in simulating the state values for the first 100 time points. After sliding window processing, when $d = 5$, 10, 15, and 20, the corresponding difference degree map sizes were 13×29, 7×15, 5×10, and 4×8. The male and female participants corresponded to two control groups, so each had two controlled time series pairs. Figure 3 shows the selection process of the optimal controlled time series pair of the female participants when the male-to-female ratio of the control group was set to 1:1. In this case, the sampling interval d was set to 20, each element in the matrix represented the functional connection difference of the BOLD series pairs between the female participant and the control group, and a smaller difference value represented the more similar brain state. The minimum value in the matrix appeared at position [1, 4]. Therefore, the corresponding empirical BOLD signals at time points 61–100 were selected as the controlled object, and the averaged NC signals at time points 101–140 were taken as the target state. Table 2 summarizes the specific controlled time series pairs in the four control settings.

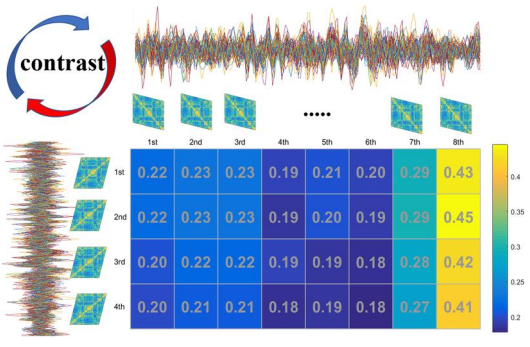

FIGURE 3 Difference between FC EMCI and FC NC of the female participant when the male-to-female ratio was set to 1:1 and $d = 20$. EMCI, early mild cognitive impairment; FC, functional connectivity.

3.2.2 | Pinning node location

The whole brain nodes were sorted in descending order according to the three centrality attributes of the structural networks. The brain regions corresponding to the top 10 network nodes with single attributes of the female and male participants are shown in Tables 3 and 4, respectively. The locations of each region in the whole brain are shown in Figure 4.[27] For the female participant, the central region was generally the same under several attributes, whereas the lentiform putamen of the male participant was in the optimal position. The reason may be that the lentiform nucleus is a part of the striatum, which is the most concentrated part of the human motor and sensory nerve conduction tracts.

We comprehensively considered the ranking and occurrence frequency of each brain region and determined the top five alternative pinning nodes for the male and female participants. For the female participant, these were identified as brain regions 73, 43, 30, 67, and 72, whereas for the male participant, they were identified as brain regions 73, 67, 43, 74, and 77. Because the number of pinning nodes would also affect the results, experiments were carried out when the number of nodes was 1, 2, 3, 4, and 5, respectively. The values of the parameters in the adaptive pinning control scheme were determined by feedback optimization, and the optimal number of pinning nodes was determined by comparing the stimulus intensity and the control effect.

TABLE 2 Specific information about the controlled time series pairs.

Sex	Female		Male	
Male to female ratio	1:1	0:1	1:1	1:0
Subject series	61–100	21–60	56–95	56–95
Controlled series	101–140	111–150	96–135	16–55

TABLE 3 The top 10 brain regions for each centrality attribute of the female participant.

Centrality attribute	1	2	3	4	5	6	7	8	9	10
Degree centrality	73	72	67	68	43	30	48	84	47	81
Betweenness centrality	73	72	67	30	43	68	81	23	48	71
Closeness centrality	73	43	30	67	72	49	36	68	71	74

TABLE 4 The top 10 brain regions for each centrality attribute of the male participant.

Centrality attribute	1	2	3	4	5	6	7	8	9	10
Degree centrality	73	67	74	85	43	83	68	84	88	5
Betweenness centrality	73	67	74	43	77	68	23	78	24	83
Closeness centrality	73	43	67	77	78	74	25	83	5	37

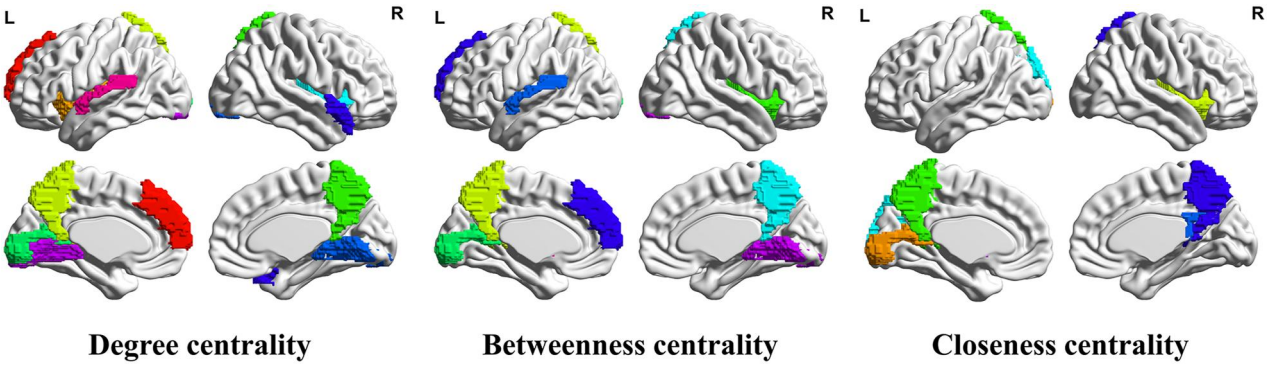

FIGURE 4 Location of the top 10 pinning nodes.

We also conducted experiments with the number of nodes set to 1, 2, 3, 4, and 5 to obtain the optimal control effect under the lowest stimulus intensity. The values of the corresponding parameters *k d i* and *c d i* (0) were determined by feedback optimization. In the experiment, the two pinning nodes, which corresponded to brain regions 73 and 43, showed better FC recovery effects for the female participant under the two control groups. When the male-to-female ratio was 1:1, the male participant had optimal results under the three pinning nodes corresponding to brain regions 73, 67, and 43, and when the male–female ratio was 1:0, the male participant got the optimal result under two pinning nodes 73 and 67 brain regions.

3.2.3 | Recovery effects of functional connectivity in the brain

Intervention experiments were conducted on the female participant in the two control settings, and better recovery results were achieved when the male-to-female ratio was 1:1. The effect of the intervention at the FC level of brain regions when the male-to-female ratio was 1:1 is shown in Figure 5A. The stimulus was applied at the 57th time point, and four brain signals were randomly selected. A significant effect of the control on the BOLD signals was observed at approximately the 83rd time point. To quantify the change in the FC strength, the FC before and after control and the averaged NC are shown in Figure 5B. After control, the FC strength between brain regions showed a significant increase in the lower right part of the FC. In general, the increase in FC intensity had significant block characteristics, and the change near the diagonal was obvious. The FCs were also compared quantitatively, and the connections that were stronger or weaker than those of the averaged NC FC are visualized in Figure 5C. The distribution of connections in the whole brain before and after control was generally uniform and consistent. Therefore, in general, the control scheme maintained the positive functions of each patient, whereas the brain regions related to negative connections changed. On the whole, the strengths of negative connections were stronger after the control. The brain regions related to negative connections before and after the control will be further analyzed.

By comparison based on Figure 6, when all brain connections were preserved, the number of connections involved in each region was almost the same before and after the control. When only the top 10% of connections were retained, a significant difference appeared. Before the control, the negative connections were evenly distributed across all brain regions. After the control, some brain region groups were highly related to the negative connections, namely brain regions 518 and 43–49. This indicates that the control scheme had a good recovery effect on the overall FC of brain regions but not on the functional recovery of the frontal, precuneus, or occipital lobes.

The male participants achieved better improvement effects than the control group with a male-to-female ratio of 1:0. Figure 7 shows the functional recovery effect of the brain area under this condition. In addition, the strength of the connection near the diagonal was significantly improved, and yellow area blocks similar to squares appeared. The cross-shaped negative blue area of the real signal became fuzzy after the intervention. Generally speaking, the functional connection matrix after the intervention was more similar to the real signal matrix, and generally, the intensity distribution developed toward the average direction of the control group. Comparing the advantageous–disadvantageous connections before and after the intervention, the strengths of some dominant connections after the intervention were higher than those before the intervention.

3.2.4 | Recovery effects of functional subnetworks

According to the analysis of the distribution of the functional connections before and after the control of the two

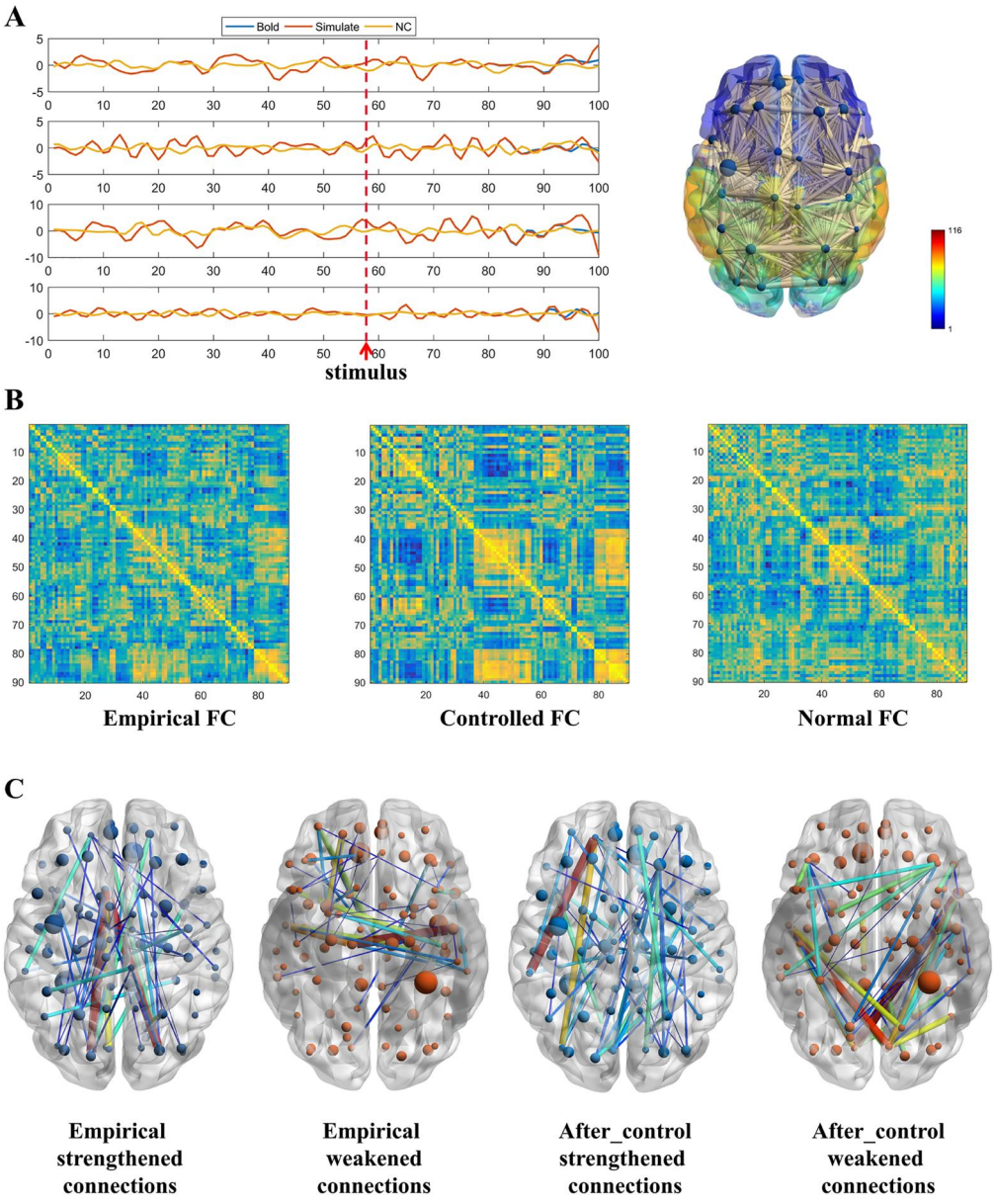

FIGURE 5 Effect of the multiple brain region collaborative control scheme on BOLD signals and FC strength of the female participant. (A) Evolution of BOLD signals in brain regions 3, 30, 50, and 72. The control was applied at the 57th time point, and the control effect was obvious after the 80th time point (left). The functional connections between the brain regions after control (right). (B) The empirical, simulated, and averaged NC FC. (C) For the strengthened and weakened functional connections before and after control, only the top 1% are displayed because of the large number. BOLD, blood oxygen level-dependent; FC, functional connectivity.

participants (Figures 8 and 9), some subnetworks were highly related to the cognitive ability of the human brain; the changes in FC within these subnetworks are further discussed in this section.

After control, the functional connection strength of all subnetworks of the female participant increased to a certain extent, which had little effect on the DAN, LN, and DMN subnetworks but caused obvious changes in the VAN and CN. This indicates that the recovery intervention can improve language comprehension, attention processing, and cognitive control in a specific individual. For the male participant, the DAN and VAN changed significantly, with the positive functional connection strength increasing. In particular, the median line of the functional connection strength distribution in the VAN was at the position of 0.6%, and 75% of brain connection strength was above 0.4.

In addition to the variation of FCs within each subnetwork, the influence of the control strategy on the communication between subnetworks was also of interest. After thresholding, the number of connections between subnetworks of the female participant before and after the control was counted (Figure 10A). No significant change was observed in the distribution of the number of connections. The maximum number of connections between

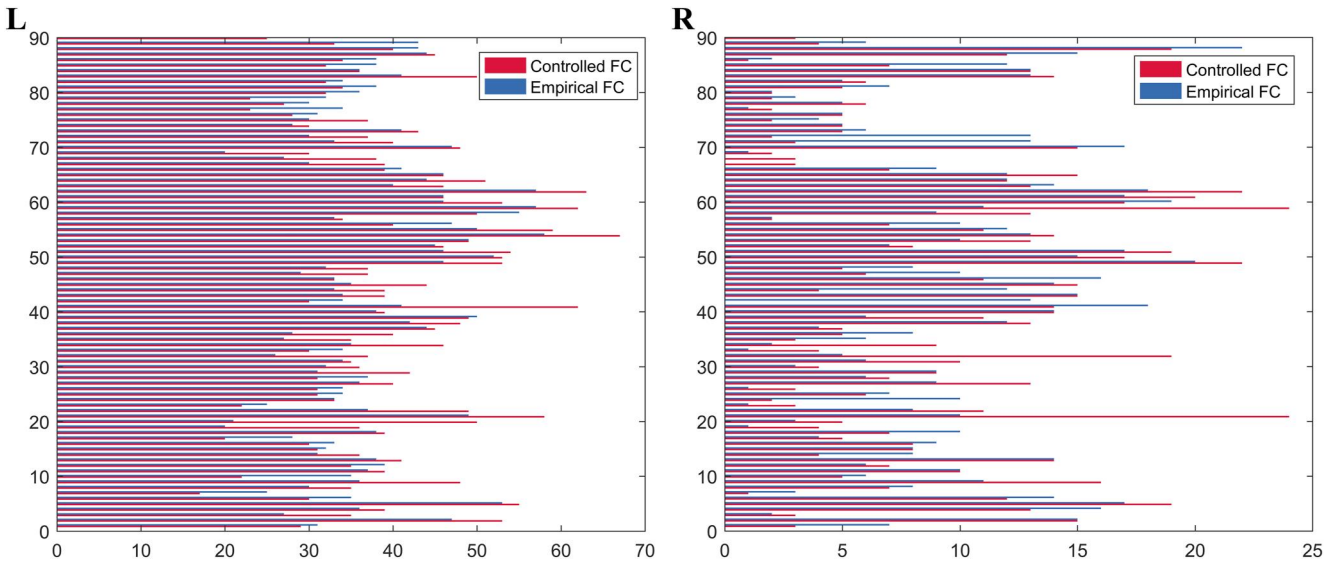

FIGURE 6 The number of weakened functional connections associated with brain regions before and after control. All connections (left), top 10% of connections (right).

the CN and DMN was maintained before and after the control, and the connections between CN and LN had the most significant increase. Furthermore, the key brain regions that play important communication roles in the above three subnetworks are also shown in Figure 10B,C; Figure 10B shows the number of connections associated with each brain region in the DMN–CN pathway, and Figure 10C shows the number of connections in the LN–CN pathway. According to the analysis shown in Figure 10B, before the control, except for some "zero-connection" brain regions, the distribution of the remaining connections was relatively uniform, and that in the DMN is more obvious. After control, the number of connections in most brain regions showed an increase, and the central position of some brain regions was more prominent, which was not obvious in the DMN. However, in the CN, brain regions 13–16 played a key role in communication with the DMN; thus, this control scheme can be considered to improve the role of the inferior frontal gyrus in information processing and transmission. In the LN–CN pathway, the control strategy caused more brain regions to participate in the information transmission of the LN–CN, and some brain regions played a central role; however, these brain regions did not show obvious aggregation, such as the brain regions 5, 42, 87 in the LN and brain regions 15, 16, 40, 61 in the CN.

In the control group with a male-to-female ratio of 1:0 (Figure 11), the number of functional connections between the DMN and LN in the male participants increased significantly. On the basis of maintaining the overall distribution, the number of connections between each group of subnetwork pairs increased significantly; the most obvious increase occurred between the CN and VAN, whereas the increase between the DMN and CN was also apparent. The CN and VAN were taken as examples for further analysis. It was found that the number of brain connections associated with the LN and DMN regions 33, 34, 41, and 42 increased from <2 to approximately 8. The obvious increase in connections in these brain regions represents the functional recovery of the amygdala and cingulate gyrus; the cingulate gyrus plays a role in regulating emotion, memory, autonomic nervous function, and motor behavior, whereas the amygdala supports the learning and memory process of the human brain. The number of connections in brain regions 11, 30, 63, and 64 related to VAN outward connections was effectively increased, namely the inferior frontal gyrus of the insula, the insula, and the superior limbal gyrus, which are the emotional control centers of the brain; the superior limbal gyrus and inferior frontal gyrus are mainly responsible for motor control. The number of connections of brain regions 9, 13, 15 and 16 associated with the CN was basically "developed from nothing." The above brain regions were found to belong to the orbital middle frontal gyrus, the triangular inferior frontal gyrus, the orbital inferior frontal gyrus, and other brain regions according to the AAL template, and the corresponding brain regions are believed to play a role in facial recognition, judging good or bad, and consequences of actions.

4 | DISCUSSION

The neural activity of the brain is the result of the complex interaction of nonlinear coupling and nonlinear oscillatory processes.[28] Therefore, we simulated BOLD signals according to a phenomenological model, that is, a single-node

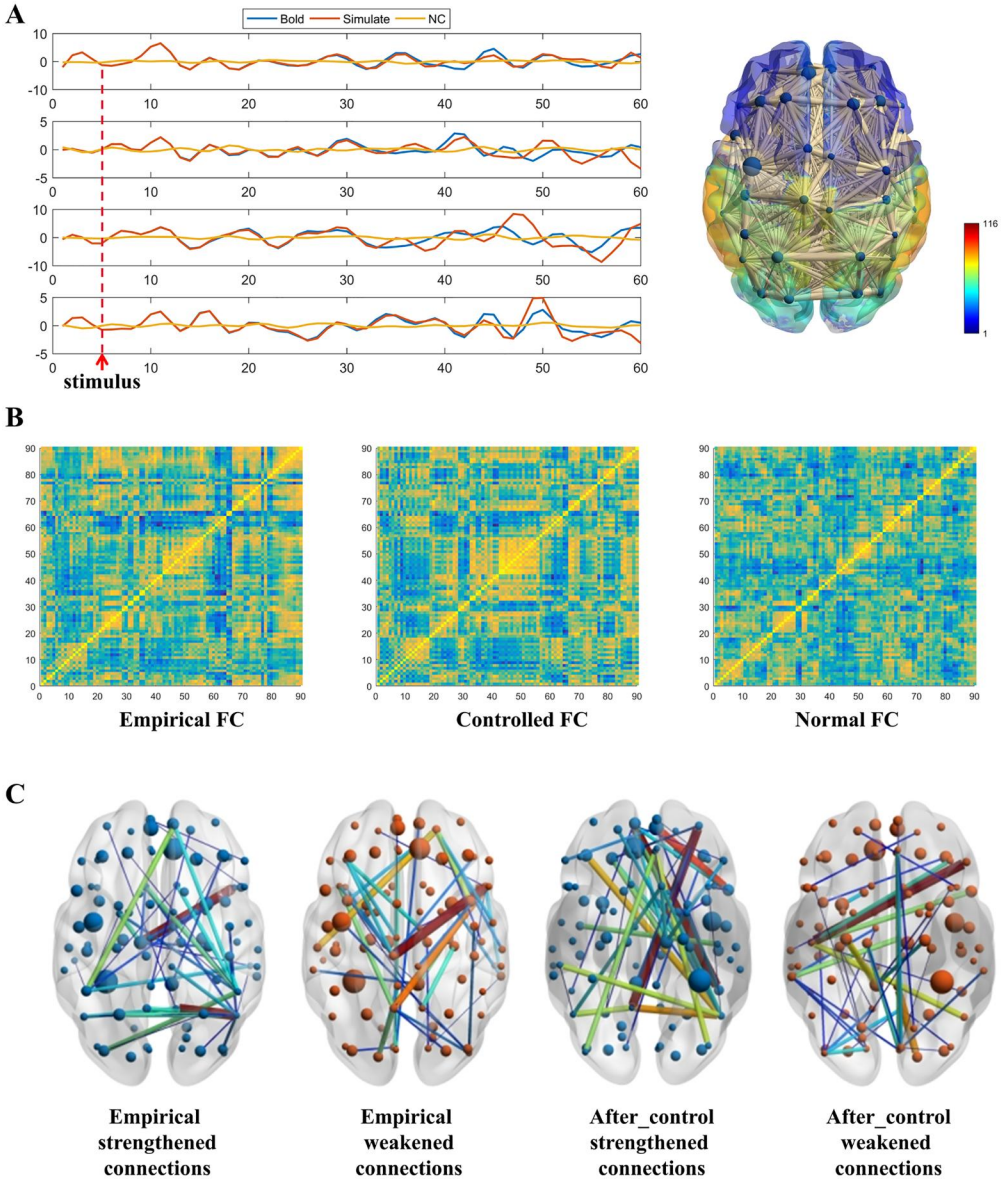

FIGURE 7 Effect of the multi-brain collaborative control scheme on BOLD signals and FC strength of the male participant. (A) The evolution of BOLD signals in brain regions 3, 30, 50, and 72. The control was applied at the 10th time point, and the control effect was obvious after the 30th time point (left). The functional connections between the brain regions after control (right). (B) The empirical, simulated, and averaged NC FC. (C) For the strengthened and weakened functional connections before and after control, only the top 1% are displayed because of the large number. BOLD, blood oxygen level-dependent; FC, functional connectivity.

dynamic equation. However, the actual coupling between regions does not appear between the hemodynamic signals but between the underlying neural activity. This method can indirectly measure changes in FC in the brain. The structural network was built on the basis of the direction of nerve bundles in the white matter, where nerve fibers gather in the brain. As nerve fibers are the constituent parts of neurons, neural activity diffuses along the structural connection network. On this basis, we determined the diffusion coefficient specific to each participant to describe the above process.

The neural activity of the human brain changes rapidly with changes in the environment and stimulation,[29] so it is difficult to obtain good applicability of a stimulation method with fixed control intensity in specific patients. The adaptive pinning control scheme can solve this problem, and its control effect is related to the selection of pinning nodes.[30,31] Clinically, patients should have as few controlled brain areas as possible. Therefore, the number of control nodes and the control energy need to be considered. This work is only a theoretical simulation; the selected brain

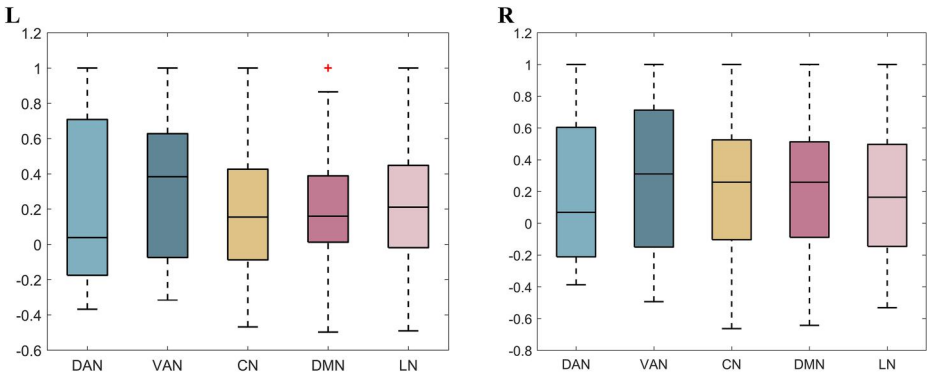

FIGURE 8 Comparison of subnetwork functional connection distribution before and after the recovery scheme of the female participant: before (left) and after (right).

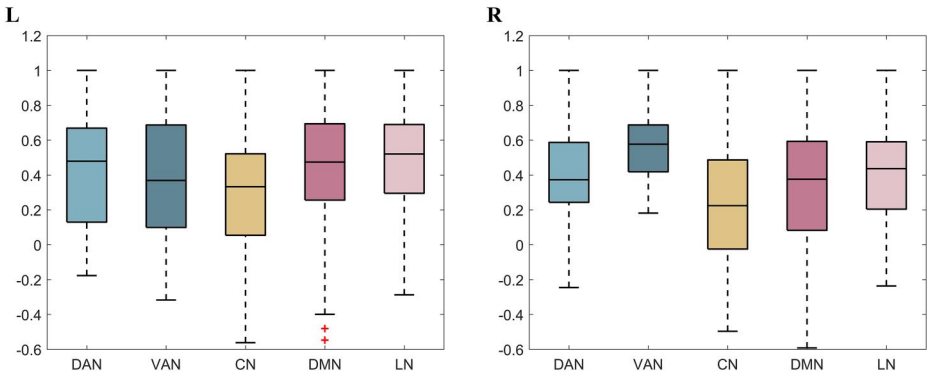

FIGURE 9 Comparison of subnetwork functional connection distribution before and after the recovery scheme of the male participant: before (left) and after (right).

regions and the determined control energy provide application ideas for clinical recovery therapy.

Considering that the BOLD signals of averaged NC are affected by a variety of external factors, directly controlling the BOLD signals of the participant so that they are consistent with the average NC can not guarantee its control effect. Therefore, finding a suitable approach to measure the similarity between FCs and locating the controlled time series pairs of the participant and the target time segment of the averaged NC can provide a more convincing explanation. In this study, the target control effect was considered so that the connection strength of several weak FCs related to cognitive ability could be improved. Therefore, the control effect had a strong correlation with the BOLD signals of the selected NC group. Ensuring that the age and other physical information of the selected NC group participants are consistent with the participants as much as possible could improve the credibility of the results.

Functional neuroimaging studies have shown that the human brain has an obvious modular structure in the large-scale functional network.[32] Some partition methods of functional modules have also been proposed. In this study, the rough partition proposed by Yeo et al. was used. Other partitioning methods include the 10 subnetworks proposed by Power et al.[33,34,35] and the 12 subnetworks proposed by Glasser et al.[36,37] To more accurately understand the influence of the control scheme on the VN and language, a system of 12 subnetworks may be more appropriate. The system of 10 subnetworks also provides a way to analyze the changes in the subcortical network. According to the different application problems, the above templates can be flexibly used to adjust the parameters of the intervention scheme and the recovery effect. In addition, in recent years, the separation and integration of functional modules have also been found to be related to the development and degeneration of human brain cognition.[38,39] Therefore, studies on brain networks have also focused on the mining integration and separation of these laws. Considering that it is suitable for discussion on a longer time scale, this study only divided the sub-network modules according to existing templates. It was also noted that although the range of connection strength in the DMN, DAN, and LN did not change significantly after control, the distribution of the connection strength in the DMN changed; therefore, it is expected that relevant cognitive abilities may also be subtly affected.

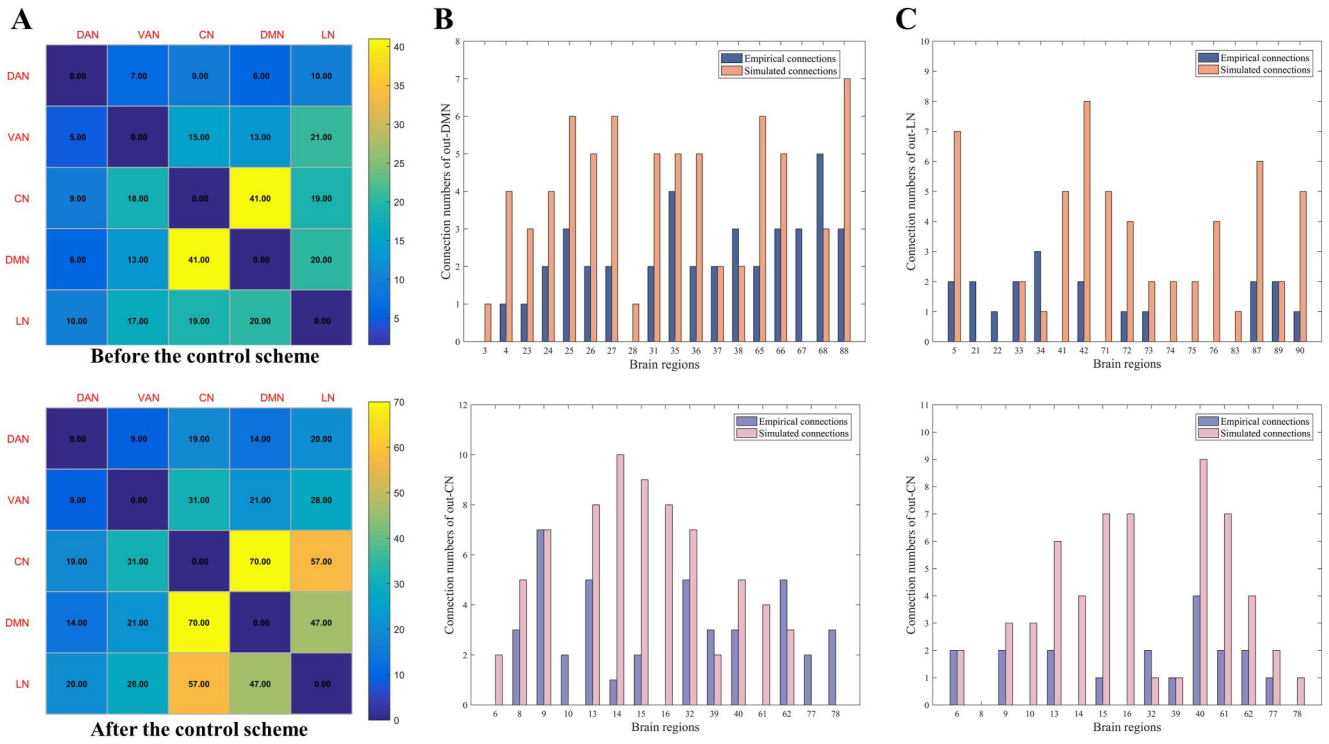

FIGURE 10 Comparison of functional connections within and between subnetworks of the female participant before and after control. (A) A comparison of the number of functional connections among subnetworks. The number of connections between the DMN and CN showed advantages, whereas the number between the LN and CN increased significantly after control. (B) Connection distribution between the DMN and CN. The distribution of DMN external connections in each brain region (top) and the distribution of CN external connections in each brain region (bottom). (C) The distribution of connections between LN and CN. CN, control network; DMN, default mode network; LN, limbic network.

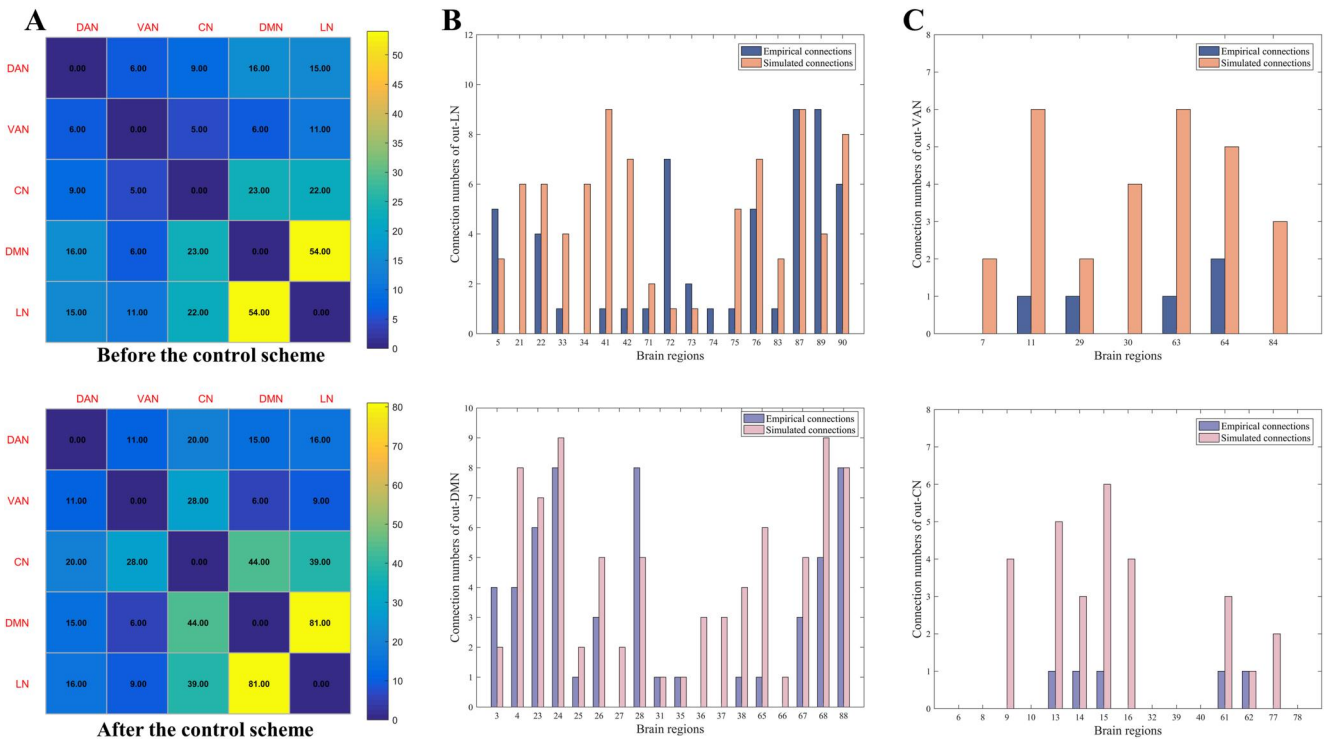

FIGURE 11 Comparison of functional connections within and between subnetworks before and after control of the male participant. (A) A comparison of the number of functional connections among subnetworks. The number of connections between the DMN and LN showed advantages, whereas the number between VAN and CN increased significantly after control. (B) Connection distribution between the DMN and LN. The distribution of the LN external connections in each brain region (top), and the distribution of the DMN external connections in each brain region (bottom). (C) The distribution of connections between the VAN and CN. CN, control network; DMN, default mode network; LN, limbic network; VAN, ventral attention network.

AUTHOR CONTRIBUTIONS

Weiping Wang: Writing – review & editing. **Haiyan Zhao**: Resources. **Chang He**: Writing – original draft. **Yuanbo Cui**: Writing – review & editing. **Zhen Wang**: Investigation. **Alexander Hramov**: Data curation. **Ping Luan**: Resources. **Xiong Luo**: Writing – review & editing. **Jipeng Ouyang**: Data curation. **Kurths Jürgen**: Writing – review & editing.

ACKNOWLEDGMENTS

This work was supported in part by a special fund for high-quality development from the Ministry of Industry and Information Technology under grant TC220A04A-182; the National Natural Science Foundation of China under grant 62271045; the National Science Fund for Distinguished Young Scholarship of China under grant 62025602; the Fundamental Research Funds for the Central Universities under grant QNXM20220038; the Key Project of Basic Research of Shenzhen under grant JCYJ20200109113603854; the Science and Technology Innovation Special Foundation of Foshan Municipal Peoples Government under grant BK21BFO01; the Innovation and Transformation Foundation of Peking University Third Hospital under grant BYSYZHKC2021107; the Key Technology Research and Development Program of Science and Technology, Scientific and Technological Innovation Team of Shaanxi Province, under grant 2020TD-013; and by the XPLORER PRIZ.

CONFLICT OF INTEREST STATEMENT

The authors declare that they have no conflicts of interest.

DATA AVAILABILITY STATEMENT

All data used to support the findings of this study are included within the ADNI (https://adni.loni.usc.edu). The raw data used to generate the figures are available from the corresponding author upon request.

ORCID

Weiping Wang https://orcid.org/0000-0002-6796-7596
Chang He https://orcid.org/0000-0001-5528-6032

REFERENCES

1. Bucci M, Chiotis K, Nordberg A; Alzheimer's Disease Neuroimaging I. Alzheimer's disease profiled by fluid and imaging markers: tau PET best predicts cognitive decline. *Mol Psychiatr*. 2021;26(10):5888-5898. https://doi.org/10.1038/s41380-021-01263-2
2. Lin Z, Huang T, Zheng G, et al. Study on the correlation between Chinese medicine syndrome and cognitive dysfunction in mild cognitive impairment. *Evid Based Complement Alternat Med*. 2022;2022:7117704-7117706. https://doi.org/10.1155/2022/7117704
3. Zhong D, Chen L, Feng Y, et al. Effects of virtual reality cognitive training in individuals with mild cognitive impairment: a systematic review and meta-analysis. *Int J Geriatr Psychiatr*. 2021;36(12):1829-1847. https://doi.org/10.1002/gps.5603
4. Feeser M, Prehn K, Kazzer P, Mungee A, Bajbouj M. Transcranial direct current stimulation enhances cognitive control during emotion regulation. *Brain Stimul*. 2014;7(1):105-112. https://doi.org/10.1016/j.brs.2013.08.006
5. Gal S, Coldham Y, Tik N, Bernstein-Eliav M, Tavor I. Act natural: functional connectivity from naturalistic stimuli fMRI outperforms resting-state in predicting brain activity. *Neuroimage*. 2022;258:119359. https://doi.org/10.1016/j.neuroimage.2022.119359
6. Ye Q, Hsieh CY, Yang Z, et al. A unified drug-target interaction prediction framework based on knowledge graph and recommendation system. *Nat Commun*. 2021;12(1):6775. https://doi.org/10.1038/s41467-021-27137-3
7. Deco G, Kringelbach ML, Jirsa VK, Ritter P. The dynamics of resting fluctuations in the brain: metastability and its dynamical cortical core. *Sci Rep*. 2017;7(1):3095. https://doi.org/10.1038/s41598-017-03073-5
8. Demirtas M, Falcon C, Tucholka A, Gispert JD, Molinuevo JL, Deco G. A whole-brain computational modeling approach to explain the alterations in resting-state functional connectivity during progression of Alzheimer's disease. *Neuroimage Clin*. 2017;16:343-354. https://doi.org/10.1016/j.nicl.2017.08.006
9. Wang D, Liang S. Dynamic causal modeling on the identification of interacting networks in the brain: a systematic review. *IEEE Trans Neural Syst Rehabil Eng*. 2021;29:2299-2311. https://doi.org/10.1109/TNSRE.2021.3123964
10. Pereira I, Frassle S, Heinzle J, et al. Conductance-based dynamic causal modeling: a mathematical review of its application to cross-power spectral densities. *Neuroimage*. 2021;245:118662. https://doi.org/10.1016/j.neuroimage.2021.118662
11. Sanchez-Rodriguez LM, Iturria-Medina Y, Baines EA, Mallo SC, Dousty M, Sotero RC. Design of optimal nonlinear network controllers for Alzheimer's disease. *PLoS Comput Biol*. 2018;14(5):e1006136. https://doi.org/10.1371/journal.pcbi.1006136
12. Kong X, Kong R, Orban C, et al. Sensory-motor cortices shape functional connectivity dynamics in the human brain. *Nat Commun*. 2021;12(1):6373. https://doi.org/10.1038/s41467-021-26704-y
13. Chen SY, Cai GQ, Liang RB, et al. Regional brain changes in patients with diabetic optic neuropathy: a resting-state functional magnetic resonance imaging study. *Quant Imag Med Surg*. 2021;11(5):2125-2137. https://doi.org/10.21037/qims-20-453
14. Jie B, Liu M, Zhang D, Shen D. Sub-network kernels for measuring similarity of brain connectivity networks in disease diagnosis. *IEEE Trans Image Process*. 2018;27(5):2340-2353. https://doi.org/10.1109/TIP.2018.2799706
15. Kirkby LA, Luongo FJ, Lee MB, et al. An amygdala-hippocampus subnetwork that encodes variation in human mood. *Cell*. 2018;175(6):1688-1700.e14. https://doi.org/10.1016/j.cell.2018.10.005
16. Strindberg M, Fransson P, Cabral J, Aden U. Spatiotemporally flexible subnetworks reveal the quasi-cyclic nature of integration and segregation in the human brain. *Neuroimage*. 2021;239:118287. https://doi.org/10.1016/j.neuroimage.2021.118287
17. Gergelyfi M, Sanz-Arigita EJ, Solopchuk O, Dricot L, Jacob B, Zenon A. Mental fatigue correlates with depression of task-related network and augmented DMN activity but spares the reward circuit. *Neuroimage*. 2021;243:118532. https://doi.org/10.1016/j.neuroimage.2021.118532
18. Northoff G, Vatansever D, Scalabrini A, Stamatakis EA. Ongoing brain activity and its role in cognition: dual versus baseline models. *Neuroscientist*. 2023;29(4):393-420. https://doi.org/10.1177/10738584221081752
19. Chao-Gan Y, Yu-Feng Z. DPARSF: a MATLAB toolbox for "pipeline" data analysis of resting-state fMRI. *Front Syst Neurosci*. 2010;4:13. https://doi.org/10.3389/fnsys.2010.00013
20. Tournier JD, Smith R, Raffelt D, et al. MRtrix3: a fast, flexible and open software framework for medical image processing and visualisation. *Neuroimage*. 2019;202:116137. https://doi.org/10.1016/j.neuroimage.2019.116137
21. Fagerholm ED, Tangwiriyasakul C, Friston KJ, et al. Neural diffusivity and pre-emptive epileptic seizure intervention. *PLoS Comput Biol*. 2020;16(12):e1008448. https://doi.org/10.1371/journal.pcbi.1008448
22. Baek EC, Hyon R, Lopez K, Finn ES, Porter MA, Parkinson C. In-degree centrality in a social network is linked to coordinated neural activity. *Nat Commun*. 2022;13(1):1118. https://doi.org/10.1038/s41467-022-28432-3

23. Eballe R, Cabahug I. Closeness centrality of some graph families. *Int J Contemp Math Sci*. 2021;16(4):127-134. https://doi.org/10.12988/ijcms.2021.91609
24. Yeo BT, Krienen FM, Sepulcre J, et al. The organization of the human cerebral cortex estimated by intrinsic functional connectivity. *J Neurophysiol*. 2011;106(3):1125-1165. https://doi.org/10.1152/jn.00338.2011
25. Jia X, Xie Y, Dong D, et al. Reconfiguration of dynamic large-scale brain network functional connectivity in generalized tonic-clonic seizures. *Hum Brain Mapp*. 2020;41(1):67-79. https://doi.org/10.1002/hbm.24787
26. Yan B, Xu X, Liu M, et al. Quantitative identification of major depression based on resting-state dynamic functional connectivity: a machine learning approach. *Front Neurosci*. 2020;14:191. https://doi.org/10.3389/fnins.2020.00191
27. Xia M, Wang J, He Y. BrainNet Viewer: a network visualization tool for human brain connectomics. *PLoS One*. 2013;8(7):e68910. https://doi.org/10.1371/journal.pone.0068910
28. Shettigar N, Yang C.-L, Tu K.-C, Suh CS. On the biophysical complexity of brain dynamics: an outlook. *Dynamics*. 2022;2(2):114-148. https://doi.org/10.3390/dynamics2020006
29. Laumann TO, Snyder AZ. Brain activity is not only for thinking. *Curr Opin Behav Sci*. 2021;40:130-136. https://doi.org/10.1016/j.cobeha.2021.04.002
30. Zhang Z, Guo R, Liu X, Zhong M, Lin C, Chen B. Fixed-time synchronization for complex-valued BAM neural networks with time delays. *Asian J Control*. 2021;23(1):298-314. https://doi.org/10.1002/asjc.2185
31. Zhang Y, Wen G, Rahmani A, Peng Z, Hu W. Cluster consensus of multi-agent systems with general linear and nonlinear dynamics via intermittent adaptive pinning control. *Trans Inst Meas Control*. 2021;43(6):1337-1346. https://doi.org/10.1177/0142331220975254
32. Liu H, Hu K, Peng Y, et al. Dynamic reconfiguration of human brain networks across altered states of consciousness. *Behav Brain Res*. 2022;419:113685. https://doi.org/10.1016/j.bbr.2021.113685
33. Power JD, Cohen AL, Nelson SM, et al. Functional network organization of the human brain. *Neuron*. 2011;72(4):665-678. https://doi.org/10.1016/j.neuron.2011.09.006
34. Cole MW, Reynolds JR, Power JD, Repovs G, Anticevic A, Braver TS. Multi-task connectivity reveals flexible hubs for adaptive task control. *Nat Neurosci*. 2013;16(9):1348-1355. https://doi.org/10.1038/nn.3470
35. Gordon EM, Laumann TO, Adeyemo B, Huckins JF, Kelley WM, Petersen SE. Generation and evaluation of a cortical area parcellation from resting-state correlations. *Cerebr Cortex*. 2016;26(1):288-303. https://doi.org/10.1093/cercor/bhu239
36. Ji JL, Spronk M, Kulkarni K, Repovs G, Anticevic A, Cole MW. Mapping the human brain's cortical-subcortical functional network organization. *Neuroimage*. 2019;185:35-57. https://doi.org/10.1016/j.neuroimage.2018.10.006
37. Glasser MF, Coalson TS, Robinson EC, et al. A multi-modal parcellation of human cerebral cortex. *Nature*. 2016;536(7615):171-178. https://doi.org/10.1038/nature18933
38. Wang R, Liu M, Cheng X, Wu Y, Hildebrandt A, Zhou C. Segregation, integration, and balance of large-scale resting brain networks configure different cognitive abilities. *Proc Natl Acad Sci USA*. 2021;118(23). https://doi.org/10.1073/pnas.2022288118
39. Tardiff N, Medaglia JD, Bassett DS, Thompson-Schill SL. The modulation of brain network integration and arousal during exploration. *Neuroimage*. 2021;240:118369. https://doi.org/10.1016/j.neuroimage.2021.118369

How to cite this article: Wang W, Zhao H, He C, et al. Target localization intervention and prognosis evaluation for an individual with mild cognitive impairment. *Brain-X*. 2023;1:e25. https://doi.org/10.1002/brx2.25